Electric-Field-Induced Perfect Anti-Nematic Order in Isotropic Aqueous Suspensions of a Natural Beidellite Clay

ARTICLE *in* THE JOURNAL OF PHYSICAL CHEMISTRY B · JUNE 2011

Impact Factor: 3.3 · DOI: 10.1021/jp201201x · Source: PubMed

7 AUTHORS, INCLUDING:

Erwan Paineau
French National Centre for Scientific Research
31 PUBLICATIONS **314** CITATIONS
SEE PROFILE

Patrick Davidson
Université Paris-Sud 11
176 PUBLICATIONS **4,492** CITATIONS
SEE PROFILE

Krassimira Antonova
Bulgarian Academy of Sciences
40 PUBLICATIONS **285** CITATIONS
SEE PROFILE

Laurent J Michot
French National Centre for Scientific Research
160 PUBLICATIONS **3,279** CITATIONS
SEE PROFILE

THE JOURNAL OF PHYSICAL CHEMISTRY B

ARTICLE

pubs.acs.org/JPCB

Electric-Field-Induced Perfect Anti-Nematic Order in Isotropic Aqueous Suspensions of a Natural Beidellite Clay

I. Dozov,[*,†] E. Paineau,[‡] P. Davidson,[†] K. Antonova,[§] C. Baravian,[∥] I. Bihannic,[‡] and L. J. Michot[‡]

[†]Laboratoire de Physique des Solides, UMR 8502 CNRS−Université Paris-Sud, Bât. 510, 91405 Orsay Cedex, France

[‡]Laboratoire Environnement et Minéralurgie, Nancy University CNRS-INPL UMR 7569, BP40, 54501 Vandœuvre Cedex, France

[§]Institute of Solid State Physics, Bulgarian Academy of Sciences, Tzarigradsko Chaussee 72, 1784 Sofia, Bulgaria

[∥]Laboratoire d'Energétique et de Mécanique Théorique et Appliquée, Nancy University UMR 7563 CNRS-INPL-UHP, 2, Avenue de la Forêt de Haye, BP160 54504 Vandœuvre Cedex, France

ABSTRACT: We study the electric-field-induced birefringence and orientational order in the isotropic phase of aqueous suspensions of exfoliated natural beidellite clay particles, thin (L = 0.65 nm) flat charged sheets with high aspect ratio, $D/L \approx 300$. Our electric birefringence experiment is optimized for aqueous suspensions of colloidal particles, with a high frequency a.c. electric field, $\nu \approx 1$ MHz, applied by two external electrodes to a thin flat sample, sealed in an optical capillary. In isotropic and biphasic samples, we observed strong field-induced birefringence $\Delta n(E)$, saturating at moderate E^{sat} field to a plateau Δn^{sat} proportional to the volume fraction ϕ. The field-induced order parameter $S(E)$ is negative and saturates to $S^{sat} = -0.5$ above E^{sat}. This corresponds to a perfect "anti-nematic" order, i.e. the normals of the beidellite particles are perpendicular to the field, without any preferred azimuthal direction. The measured specific excess polarizability ΔA^{sp} is among the highest data reported for other strongly anisometric dielectric and metal particles. We explain the high ΔA^{sp} value with the strong induced polarization of the electric double layer of counterions at the charged particle/electrolyte interface. The estimated equivalent conductivity of the beidellite particle $K^{eq} = 2K^{\sigma}/L$ is several orders of magnitude larger than the bulk conductivity of the electrolyte K_e, resulting in a metal-like behavior of the beidellite disks under field. In the isotropic regions of biphasic nematic/isotropic samples, the excess polarizability is further enhanced by an order of magnitude, indicating collective reorientation of the particles. We propose that this enhancement might be due to pretransitional fluctuations of the spontaneous nematic order S_N of the colloidal suspension and/or formation of chains of particles, with antinematic order of the beidellite disks in the chains.

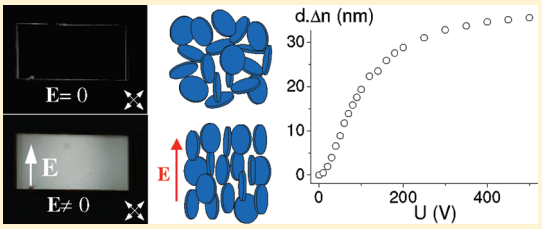

INTRODUCTION

Swelling clay minerals are naturally occurring charged aluminosilicates that are one of the main mineral constituents of soils. When exchanged with monovalent cations, they can fully delaminate in low ionic strength aqueous suspensions, where they are then present as single layers with high aspect ratio (typical equivalent diameters of a few hundreds of nanometers for a thickness of less than one nanometer). This feature is used in numerous industrial applications[1,2] that take advantage, in particular, of the fact that such suspensions gel at very low volume fractions. For volume fractions below the sol/gel transition, one may, however, expect natural swelling clay minerals to display an isotropic/nematic (I/N) phase transition. The existence of such a transition has been debated for decades since Langmuir's seminal paper.[3] In recent years, some progress was made in this respect, as three different natural swelling clay minerals have been shown to exhibit an unequivocal I/N transition at low ionic strength.[4−7] These three minerals (two nontronites and one beidellite) are true mineral liquid crystals[8,9] made up of bidimensional particles and can then be studied using techniques classically used for organic thermotropic and lyotropic liquid crystals. In that framework, the application of external fields to the particles is of prime importance, for both fundamental interest and possible development of liquid-crystal devices based on natural materials.

The present study is focused on beidellite, a tetrahedrally charged swelling clay mineral with aluminum in the octahedral layer whose phase diagram at low ionic strength exhibits, with increasing volume fraction, an isotropic phase, a biphasic region and a nematic liquid phase before the sol/gel transition.[7] Due to its high aspect ratio, such a mineral should exhibit a strong anisotropy of electric susceptibility. In this context, measuring electric birefringence is a classical method[10−16] to study the field-induced orientation of anisotropic colloidal particles or molecules, respectively in colloidal suspensions or molecular liquids and macromolecular solutions. The typical Kerr cell,[17−22] used in the large majority of the experiments, consists of two long flat electrodes ($L_e \approx 2-10$ cm) immersed in the liquid and a few

Received: February 5, 2011
Revised: May 1, 2011
Published: June 01, 2011

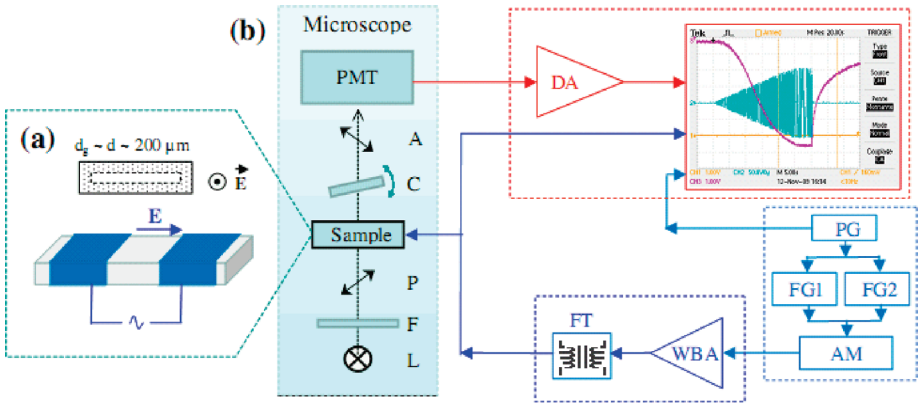

Figure 1. Experimental setup. (a) Electro-optic cell in a thin flat optical capillary; (b) block scheme of the measurement apparatus.

millimeters apart. Up to several kV of d.c. or a.c. voltage is applied to the electrodes, providing a strong and uniform electric field in the liquid. The field-induced orientation is then measured from the phase shift of a collimated polarized light beam, propagating parallel to the electrodes. The long optical path ($\sim L_e$) of the Kerr cell insures a high sensitivity in terms of the measured birefringence, enabling to work with very low volume fractions ($\phi \approx 10^{-5}$) and/or "weak" fields (10−100 V/mm). On the other hand, due to the direct contact between the electrodes and the electrolyte and to the strong current in the Kerr cell, a number of parasitic phenomena take place: polarization and Faradaic reactions on the electrodes lead to fast sample degradation; convective flows due to electrokinetic phenomena and Joule heating give spurious birefringence signals through flow alignment of the particles; the light scattering and absorption, integrated over the long optical path of the probe beam, are difficult to separate from the induced birefringence signal.

In the present study, we are interested in relatively large volume fractions ($\phi \approx 10^{-3}$ to 10^{-2}), covering the isotropic, biphasic and nematic regions of the phase diagram of the suspensions of beidellite clay particles. To minimize the parasitic effects and to observe directly the textures of the spontaneous or field-induced liquid-crystal phases, we developed an original experimental setup,[7] inspired by the electro-optical studies in thermotropic liquid crystals.[23−26] Through a detailed study of the evolution of birefringence with applied field, we show that the electrically induced nematic order parameter in aqueous suspensions of beidellite clay is negative and extremely high, similar to the expected one for metal particles with the same aspect ratio, immersed in an insulating liquid. In a simple model, we show that the observed strong field effect is due mainly to the polarization of the ionic atmosphere around the charged beidellite particles.

MATERIALS AND METHODS

Preparation of Beidellite Clay Suspensions. Beidellite is a natural dioctahedral swelling clay mineral with a charge deficit located in the tetrahedral sheet, resulting from the substitution of Si by Al. Samples of natural beidellite SBId-1 were purchased from the Source Clays Minerals Repository of the Clay Mineral Society at Purdue University. Clay suspensions were purified following already described procedures.[4−7] After grinding the raw sample, a 40 $g \cdot L^{-1}$ clay suspension was exchanged three times in 1 M NaCl solution during 24 h. Excess chloride was then removed by dialyzing the suspension against Milli-Q water until the conductivity was below 5 μS/m. After recovery from the dialysis tubes, the suspension was then transferred into Imhoff cones and was left to sediment during 24 h. The supernatant was then siphoned off as the bottom of the cone contains miscellaneous impurities (mainly sand-size quartz, feldspar and iron and titanium oxyhydroxydes) that were discarded. In order to reduce polydispersity, size fractionation procedures were then applied. The stock suspension was first centrifuged at 7000*g* during 90 min. The sediment was collected, rediluted in Milli-Q water, and will be referred to as "size 1" hereafter. The same procedure was then applied after centrifugations at 17000*g* and 35000*g* thus yielding "size 2" and "size 3" fractions, respectively. The size of individual particles was determined by transmission electron microscopy (TEM) using a CM12 Philips microscope operating at 80 keV. The samples used in the present study correspond to size 3 beidellite with an average diameter of 210 nm[7], the thickness of the individual clay layers being around 0.65 nm.

In order to scan the whole (volume fraction/ionic strength) phase diagram, homogeneous suspensions were prepared by osmotic stress. Diluted beidellite suspensions were then placed in dialysis tubes (Visking, molecular weight cutoff 14000 Da) immersed in PEG 20000 solutions of fixed ionic strength. At the end of the experiment, the beidellite suspensions were recovered and their mass concentrations were determined by weight loss upon drying.

Electro-Optic Setup and Technique. Our experimental setup is presented schematically in Figure 1. The colloidal suspension was filled into a thin flat optical capillary (VitroCom, NJ) of typical internal cross section $d \times w = 0.2 \times 2.0$ mm^2 (Figure 1a). The capillary was then flame-sealed to avoid water evaporation. A high frequency a.c. electric field was applied to the colloid along the capillary axis, by using two external electrodes. These are flat rings of aluminum foil wrapped around the capillary and separated by a distance $l = 1$ mm. The capillary can be inserted into the electrodes and then freely translated, which allows choosing the observation area during the experiment, an important feature in the cases of surface-induced order in the colloid, spontaneously anisotropic textures, and biphasic samples.

For the electro-optic experiment, the sample was placed on the stage of a Leitz Ortholux polarizing microscope, housing all the optical parts of the setup (Figure.1b): a lamp L with stabilized d.c. power supply; interference filter F ($\lambda = 546$ nm); polarizer P and analyzer A, crossed at ±45 to the field direction; tilting (Berek) optical compensator C; and a photomultiplier tube PMT,

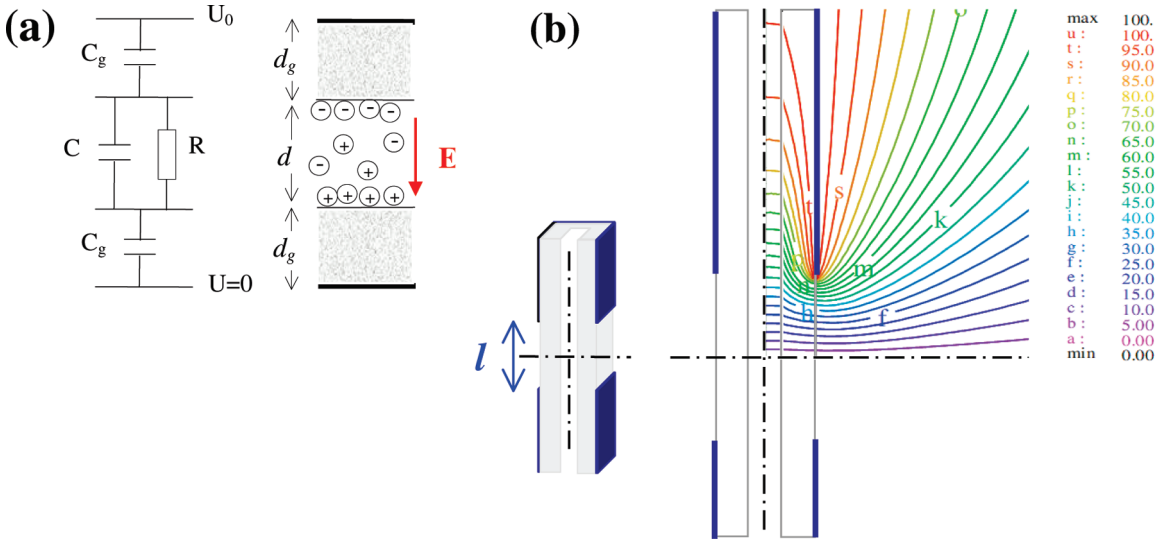

Figure 2. Field penetration in the sample. (a) Equivalent electric circuit for a simple flat sandwich geometry of the cell; (b) equipotential surfaces in the sample, obtained by numerical resolution of the Laplace equation in the actual cell geometry (to simplify, only one quadrant is shown on the figure).

equipped with variable observation window defined by two slits (Leitz). Using the compensator provides a direct visual measurement of the induced birefringence, rather insensitive to light scattering and dichroism artifacts. Indeed, the measure does not depend on the absolute transmitted light intensity, but only on the position of the zero-order interference band minimum. In PMT measurement mode, the compensator introduces a controlled phase shift δ_c, most often $\delta_c = \lambda/4$, superposed to the optical path difference δ introduced by the sample birefringence Δn, $\delta = d\Delta n$. This insures a high sensitivity and a quasi-linear response of the transmitted light intensity $I(\delta)$ for $\delta \ll \lambda/4$

$$I(\delta) = I_0 \sin^2\left[\frac{\pi}{\lambda}(\delta_c + \delta)\right] \cong \frac{1}{2}I_0 + \frac{\pi}{\lambda}I_0\delta \quad (\text{at } \delta \ll \delta_c = \lambda/4) \tag{1}$$

where I_0 is the maximum of the transmitted intensity, measured at $\delta + \delta_c = \lambda/2$.

The signal applied to the sample was a high frequency ($\nu \approx 1$ MHz) sinusoidal voltage $U = U_0 \cos(2\pi\nu t)$, either continuous or pulsed, with controlled pulse duration and envelope shape. The signal generation block consists in a pulse generator PG, used as a "clock" to synchronize all the other instruments, a couple of function generators, FG1 and FG2, synthesizing respectively the high frequency sinusoidal field and the envelope $U_0(t)$, and an amplitude modulator AM mixing these two signals.

The resulting low-voltage (U_0 < 10 V) signal is sent to the amplifying block, consisting of the commercial wide-band amplifier WBA (Krohn-Hite 7602M) and an optional homemade ferrite-core transformer FT, providing up to U_0 = 700 V on the sample, and to the first channel of the oscilloscope (e.g., the green trace that linearly increases in time shown on Figure 1b).

The signal from the PMT, proportional to the measured phase-shift (apart from the constant $I_0/2$ term), is sent to the differential amplifier DA (Tektronix, TDS 2004B). It works in a comparator mode, removing the irrelevant constant component, filtering the high-frequency noise, and amplifying the signal up to 10^3 times. Finally, the signal is sent to the digital oscilloscope DO and accumulated there up to 128 times to decrease the low-frequency noise without slowing down the time response of the system. As example, the magenta trace in Figure 1b shows the time-dependent signal, proportional to the instantaneous value of the birefringence, induced by the slowly increasing applied field (green trace).

The capillary glass wall, separating in our cell the electrodes from the colloid, prevents electrolysis and other sources of sample degradation. However, it also seriously affects the field penetration in the sample. In a first approximation, valid for simple geometries like the one sketched on Figure 2a, the effective rms value E of the field inside the suspension can be written as[7]

$$E = c_d c_s(\nu)\frac{U_0}{\sqrt{2}l} \tag{2}$$

where the coefficients c_d and $c_s(\nu)$ are correction factors for the field attenuation in the sample, due respectively to the dielectric mismatch of the glass ($\varepsilon_g \approx 4$) with the electrolyte ($\varepsilon_e \approx 80$) and to the screening of the field arising from charge accumulation on the wall/suspension interface.

Qualitatively, we can obtain the correction factors for the field penetration in the sample from the simple equivalent electric circuit, presented on Figure 2a for a flat sandwich cell geometry (differing from the actual geometry of our cell by the direction of the electric field). The field inside the sample drives the mobile charges of the electrolyte toward the electrodes. At the wall/suspension interface, the ions are stopped and build up an electric double layer, decreasing the field in the liquid. At low enough frequency, the ions move in phase with the applied field and the charges accumulate until the field is completely screened in the bulk electrolyte: the screening coefficient becomes $c_s(\nu) \approx 0$ and the effective field in the sample is then negligible. When the frequency ν increases toward the charge relaxation frequency[27,28] of the suspension $\nu_c = K_e/(2\pi\varepsilon_0\varepsilon_e)$, defined by the suspension conductivity K_e and the dielectric constant ε_e of the electrolyte, the charge carriers lag behind the field and the screening is only partial. Finally, at $\nu \gg \nu_c$, the charge accumulation during the half-period of the field is negligible and the field penetrates the sample without any screening, $c_s(\nu) \approx 1$. From the equivalent

dx.doi.org/10.1021/jp201201x |J. Phys. Chem. B 2011, 115, 7751–7765

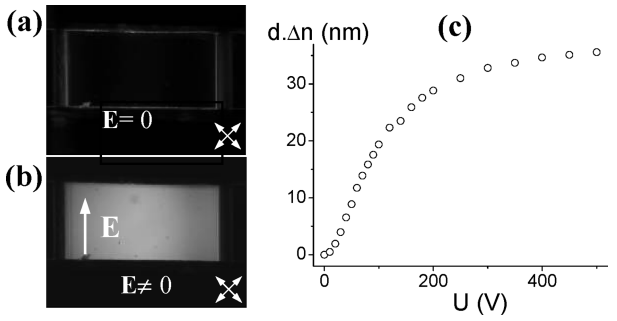

Figure 3. Electric birefringence in the isotropic phase of beidellite clay suspension ($\phi = 4.1 \times 10^{-3}$). Microphotographs of the sample between crossed polarizers (the white arrows at 45° to the field direction) before (a) and after (b) the application of the field (ν = 500 kHz, amplitude of the applied voltage U_0 = 140 V). (c) phase-shift in the cell (optical path length d = 200 μm) measured as a function of the applied rms voltage $U = U_0/\sqrt{2}$.

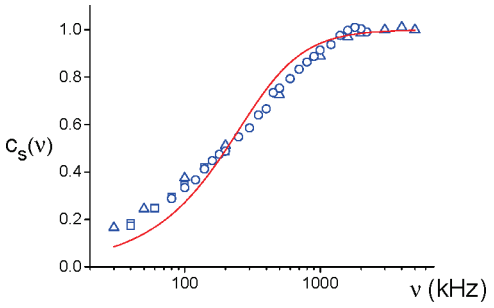

Figure 4. Frequency dependence of the screening coefficient $c_s(\nu)$ measured at ionic strength of the electrolyte 10^{-4} M/L. The different symbols correspond to measurements with different fixed levels of the internal field E in the sample. The solid line is the best fit with eq 3, giving ν_c = 430 kHz.

electric circuit of the simple ideal geometry sketched on Figure 2a, the screening coefficient $c_s(\nu)$ can be calculated analytically[28,29]

$$c_s(\nu) = \frac{\nu}{\sqrt{\nu^2 + \nu_c^2}} \qquad (3)$$

For the more complicated real geometry of our cell, $c_s(\nu)$ can be obtained numerically. However, as we have direct experimental access to the screening coefficient (see the Experimental Results section), we use in practice the measured $c_s(\nu)$ dependence for the recalibration of the field in the sample.

The second important field-attenuation factor, the c_d coefficient in eq 2, is related to the voltage drop across the two glass wall capacitances C_g in the equivalent circuit. For the flat sandwich cell of Figure 2a, these capacitances are in series with the much larger capacitance of the suspension $C \approx C_g \cdot (\varepsilon_e d_g)/(\varepsilon_g d)$. For aqueous suspensions, this results in extremely weak penetration of the field in the electrolyte, $c_d \approx 1/40 \ll 1$ (however, as recently demonstrated,[30] this geometry remains quite useful in the case of a moderate dielectric constant of the solvent, or even for aqueous suspensions in the case when the electrodes are in direct contact with the electrolyte[31,32]). On the contrary, in the actual geometry of our cell, with the field parallel to the glass/liquid interface, the two C_g capacitors are, roughly speaking, in parallel with C. The coefficient c_d drastically increases and the field penetrates in the suspension much more efficiently. Figure 2b shows the equipotential surfaces, and hence the field distribution in the sample, obtained by a numerical solution of the Laplace equation[33] in our cell geometry ($d = d_g$ = 200 μm, l = 1 mm). As it can be seen from the figure, in the interelectrode area of interest, the field in the sample is relatively strong ($c_d \approx 0.41$), parallel to the capillary axis and highly uniform (less than 3% variation). In the following, we use this calculated c_d value to estimate the effective rms field E in the suspension.

EXPERIMENTAL RESULTS

Before the electric birefringence measurements, the capillaries filled with samples of beidellite suspensions were stored vertically for a few days. For volume fractions $\phi < 4.2 \times 10^{-3}$, corresponding to the isotropic phase, the samples homogenize during storage and relax from spurious birefringence due to flow alignment and surface-induced orientation. For the samples in the biphasic region of the phase diagram, with $4.2 \times 10^{-3} < \phi < 5.9 \times 10^{-3}$, a phase separation takes place in the capillary, with the usual growth and sedimentation of "tactoid" nematic droplets.[34,35] After a few weeks, two continuous regions are observed, isotropic at the top and nematic at the bottom and their proportion does not significantly change any further. Moreover, no particle sedimentation could be detected in any of the capillaries. All electric birefringence measurements presented here were made in the isotropic region, with no tactoids and far away from the adjacent nematic phase.

Without field, the sample observed between crossed polarizers appears dark (Figure 3a), as expected for the isotropic phase. A small spurious phase-shift, due to the residual stress birefringence of the capillary glass walls, of typically 2−4 nm, is measured at $E = 0$ and the data under field are corrected for this artifact. Under increasing field (Figure 3b), the transmission increases, due to the orientation of the particles and the field-induced nematic-like order. The field-induced optical anisotropy is uniaxial and positive, i.e. the slow axis is parallel to the field, along the capillary axis. The typical dependence of the phase-shift $d\Delta n$, measured as a function of the applied rms voltage at fixed frequency ν = 500 kHz, is shown on Figure 3c. The usual Kerr regime is observed at low voltage and the birefringence increases as U^2. However, at U > 50 V, the curve deviates from the Kerr regime and rapidly saturates toward a finite $d\Delta n^{sat}$ value.

Because the birefringence is a function of the internal field in the suspension, it can be used as an in situ probe to study the field penetration in the sample. Local measurement of the slow axis orientation and the phase-shift over 20 × 20 μm^2 area, while scanning over the whole interelectrode region, confirms that the field in the sample is rigorously parallel to the capillary axis and of uniform strength (less than 3% variation), as predicted by the finite element numerical simulation. The curves $\Delta n(U)$, measured at different frequencies, differ only by a scaling factor of the voltage axis, as expected from eq 2.

Supposing that $c_s(\nu)$ saturates toward $c_s(\nu) \approx 1$ at the highest frequencies accessible with the present setup, and measuring the voltage $U(\nu)$ needed to obtain the same birefringence, and hence the same internal field, we obtain the screening coefficient $c_s(\nu)$ plotted on Figure 4. The experimental curve is in qualitative agreement with eq 3, giving a charge relaxation frequency ν_c = 430 kHz for the electrolyte, compatible with the value ν_c = 660 kHz estimated from the experimentally measured conductivity $K_e \approx 3 \times 10^{-3}$ S/m of the suspension. The perfect saturation of

dx.doi.org/10.1021/jp201201x |J. Phys. Chem. B 2011, 115, 7751–7765

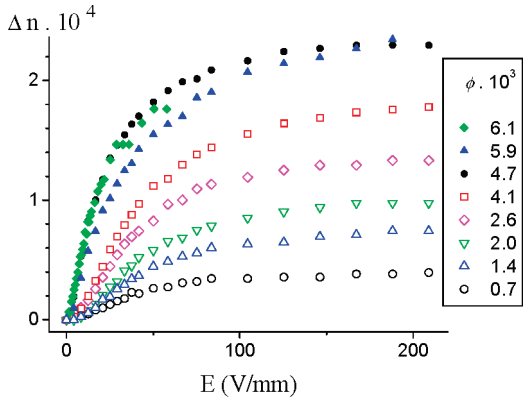

Figure 5. Induced birefringence $\Delta n(E)$ as a function of the rms value E of the electric field inside the sample for different volume fractions ϕ of the beidellite particles (ionic strength 10^{-5} M/L, ν = 500 kHz). The open and full symbols refer respectively to isotropic and biphasic samples.

$c_s(\nu)$ above $\nu \approx 2$ MHz shows that there are no additional relaxation processes at higher frequencies in the accessible $\nu < 5$ MHz range. All the following experiments were performed at fixed frequency in the range 0.5 − 1.0 MHz, ensuring the best compromise between an effective field penetration in the sample and a maximal $U_0(\nu)$ amplitude accessible with our apparatus.

Strictly speaking, the factorization of the two correction coefficients in eq 2 and the simple result for $c_s(\nu)$ given in eq 3 are exact only in the case of a flat sandwich geometry of the sample. To avoid the errors introduced by this approximation in the estimated internal field in the electrolyte, we use, in the data interpretation, eq 2 with the numerically calculated $c_d \approx 0.41$ correction factor (exact result for $\nu \gg \nu_c$, i.e., in the plateau region of Figure 4) and the experimentally measured $c_s(\nu)$ coefficient (which takes exactly into account the frequency dependence in the actual geometry of the experiment).

The induced birefringence $\Delta n(E)$ is presented on Figure 5 as a function of the rms value of the electric field E inside the sample for different volume fractions ϕ of the beidellite particles (ionic strength 10^{-5} M/L, similar results were obtained for the 10^{-4} M/L series of samples). Open and full symbols refer respectively to the isotropic and the biphasic domains of the phase diagram, but the regions under study are isotropic in both cases. Note that our experiment is sensitive to the local volume fraction ϕ_{loc} in the region under study. For the isotropic samples, ϕ_{loc} coincides with the overall volume fraction ϕ defined by the preparation of the suspensions. After the phase separation of the biphasic samples, however, the local volume fractions in the coexisting isotropic and nematic phases are respectively $\phi_{loc} = \phi_I \approx 4.2 \times 10^{-3}$ and $\phi_{loc} = \phi_N \approx 5.9 \times 10^{-3}$, different from the ϕ value reported in the caption of Figure 5. Therefore, the full-symbol curves correspond to essentially the same $\phi_{loc} = \phi_I$ and are clustered together. In the following, we will systematically plot our results against ϕ_{loc} instead of ϕ, to take into account the equilibrium value of the volume fraction in the studied region.

For all volume fractions, the curves on Figure 5 show similar behavior, with initial quadratic increase (Kerr regime) limited to very weak fields $E < 30$ V/mm. At higher fields, the birefringence progressively saturates to a ϕ-dependent plateau $\Delta n^{sat}(\phi)$. Qualitatively, a similar behavior has been reported[36−43] for many other isotropic colloidal suspensions, consisting of very large and highly anisotropic particles. However, the low values of the saturation field observed here are quite untypical for particles of moderate volume V^P, which shows an unusually strong coupling of the beidellite sheets with the field.

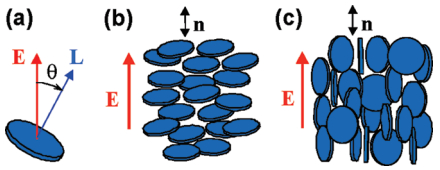

Figure 6. Orientational order of disk-like particles under field. The macroscopic symmetry axis of the induced order is the nematic director $\mathbf{n} \| \mathbf{E}$. (a) Definition of the angle θ between the field $\mathbf{E}$ and the symmetry axis of the particle $\mathbf{L}$. (b) Strong positive induced order $S(E) \approx 1$ for the case $\Delta A > 0$. (c) Strong negative induced order $S(E) \approx -1/2$ for $\Delta A < 0$, the usual case for disk-like particles.

For low volume fractions, the particles can be considered as independent, and the induced birefringence is approximately additive[36,44]

$$\Delta n(E) = \Delta n^P \phi S(E) \tag{4}$$

where Δn^P is the specific average optical anisotropy of the particles, i.e., when the birefringence is extrapolated to $\phi = 1$ and for a perfectly oriented system ($S = 1$). All of the information about the particle orientation in the field is contained in the induced orientational order parameter $S(E)$, related to the average orientation of the particle symmetry axis $\mathbf{L}$ respective to the field direction (Figure 6)

$$S(E) = \frac{1}{2}\langle 3\cos^2\theta - 1\rangle = \frac{1}{2}\int_0^1 f(\theta)(3\cos^2\theta - 1)d\cos\theta \tag{5}$$

where

$$f(\theta) = \exp(-U^P(\theta)/kT)/\int_0^1 \exp(-U^P(\theta)/kT)d\cos\theta \tag{6}$$

is the orientational distribution function of the particles under the field action and $U^P(\theta)$ is the interaction energy of the particle with the electric field.

For the high frequency a.c. field used here, typically ν = 500 kHz, we can neglect the terms in $U^P(\theta)$ which are linear in E and related to the reorientation of the permanent dipole of the particle:[36,45] such terms are averaged to zero because the particle cannot follow the field inversion at this time scale. Then, $U^P(\theta)$ is quadratic in E and its most general form is

$$-\frac{U^P(\theta)}{kT} = \frac{1}{2}\mathbf{E}\cdot\mathbf{A}\cdot\mathbf{E} = \text{const.} + \frac{1}{2}\Delta A E^2\cos^2\theta \tag{7}$$

Here, the tensor $\mathbf{A}$ describes the anisotropic coupling of the particle orientation with the applied field. In the particle reference frame, $\mathbf{A}$ is diagonal, with eigenvalues $A_\|$ and $A_\perp$ (we assume a cylindrical symmetry for the particle). The physical meaning of $\mathbf{A}$ is the excess of polarizability of the particle, compared to the surrounding medium (and renormalized with kT). The sign and the strength of the relevant coupling coefficient $\Delta A = A_\| - A_\perp$, the anisotropy of the particle excess polarizability, control the particle behavior under field. For strong fields, $E^2 \to \infty$, the

dx.doi.org/10.1021/jp201201x | J. Phys. Chem. B 2011, 115, 7751–7765

induced order parameter $S(E)$ saturates either to $S^{sat} = 1$ (Figure 6b, $\Delta A > 0$, usual situation for prolate particles) or to $S^{sat} = -1/2$ (Figure 6c, $\Delta A < 0$, usual situation for oblate particles).

Strictly speaking, the approximation in eq 4 is valid only for infinitely dilute systems. For dense systems, the average optical susceptibility is no more additive, due to the interference of the optical fields emitted by the close-by particles. However, from the birefringence measurements in the nematic phase of the suspensions, aligned by strong magnetic or electric fields,[7] we obtain $\Delta n^P = -0.09 \pm 0.007$. This rather small value is confirmed qualitatively by calculation with the Peterlin−Stuart formula[44] from the known axial ratio of the particles and the literature data for the optical indices of the beidellite. The weak optical anisotropy of the beidellite particles justifies the use of eq 4 for the moderate ϕ values of the suspensions under study. However, at the applied electric field frequency ν, the dielectric anisotropy of the particles is much stronger. This should be taken into account by additional (ϕ dependent) terms in the energy (7), resulting in ϕ dependent coupling coefficient $\Delta A(\phi)$, increasing at high volume fractions, especially as one approaches the isotropic−nematic transition.

On Figure 7 are presented the saturated values of the birefringence $\Delta n^{sat}(\phi)$, obtained from an extrapolation of the measured $\Delta n(E)$ curves to $E^2 \rightarrow \infty$. The result is in good agreement with the linear dependence predicted by eq 4, keeping in mind that the local volume fraction in the biphasic samples (full symbols) is $\phi_{loc} = \phi_I = 4.2 \times 10^{-3}$, the thermodynamic equilibrium value for the isotropic phase in coexistence with the nematic phase. At the saturation, eq 4 reduces to $\Delta n^{sat}(\phi) = \Delta n^P \phi S^{sat}$, giving for the saturated order parameter $S^{sat} = \Delta n^{sat}(\phi)/(\phi \Delta n^P) = -0.51 \pm 0.03$, in excellent agreement with the theoretical limit $S^{sat} = -1/2$ for a perfectly ordered phase of oblate particles.

Figure 8 displays the field-induced order parameter $S(E) = S^{sat}\Delta n(E)/\Delta n^{sat}(\phi)$ obtained by renormalization of the electric birefringence data for the two series of samples, with ionic strengths 10^{-5} and 10^{-4} M/L respectively. For $\phi < 0.2\%$, far from the isotropic/nematic transition, the curves are close together, showing that the induced order is mainly due to the individual reorientation of the particles, and not to their interactions. For higher volume fractions, the order increases faster at weak or moderate fields, enhanced by the nematic fluctuations, i.e. by collective effects arising from the increasing steric interactions between the particles. On the same figure are presented (solid lines) the best fits of the low-ϕ curves with eqs 5−7, giving fairly large values for the coupling coefficients, $\Delta A_{exp}(\phi \rightarrow 0) = -3.7 \times 10^{-9}$ and -2.5×10^{-9} m^2 V^{-2} respectively. The best fit curves at low field for the biphasic samples (dashed lines) show additional enhancement by 1 order of magnitude of the coupling coefficients $\Delta A_{exp}(\phi_I) = -3.2 \times 10^{-8}$ and -1.8×10^{-8} m^2 V^{-2} respectively, due to the collective reorientation of the particles and the strong interactions between them. Qualitatively, the experimental results on Figure 8 are very similar for the two

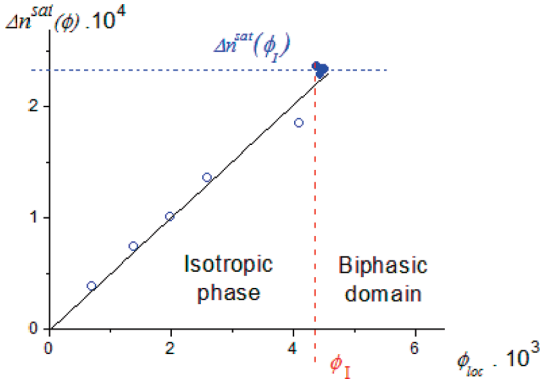

Figure 7. Saturated values of the birefringence $\Delta n^{sat}(\phi)$ measured in isotropic (open symbols) and biphasic (full symbols) samples with ionic strength 10^{-5} M/L. The data are plotted as a function of the local volume fraction in the measured isotropic regions.

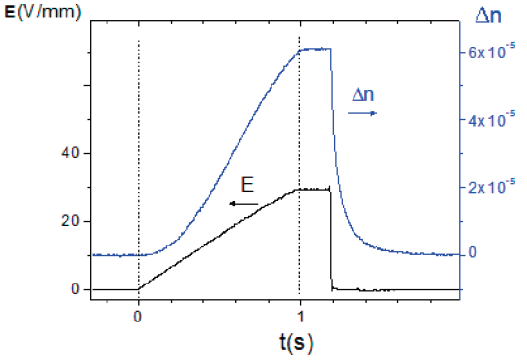

Figure 9. Shapes of the applied pulse $E(t)$ and birefringence signal $\Delta n(t)$ following adiabatically the field (ionic strength 10^{-4} M/L, $\phi = 0.0033$).

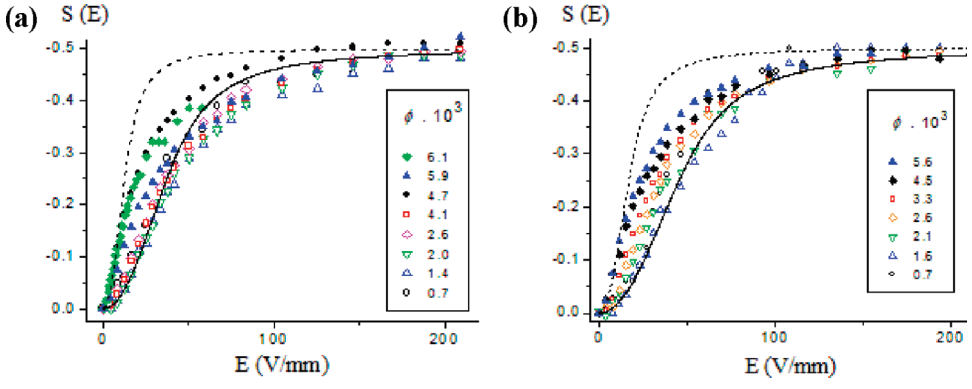

Figure 8. Field induced order parameter $S(E)$ of the beidellite suspensions with ionic strength (a) 10^{-5} and (b) 10^{-4} M/L. The solid and dashed-line curves are the best fits with eqs 5−7, respectively, for volume fractions far away and close to the isotropic/nematic phase transition.

dx.doi.org/10.1021/jp201201x |J. Phys. Chem. B 2011, 115, 7751–7765

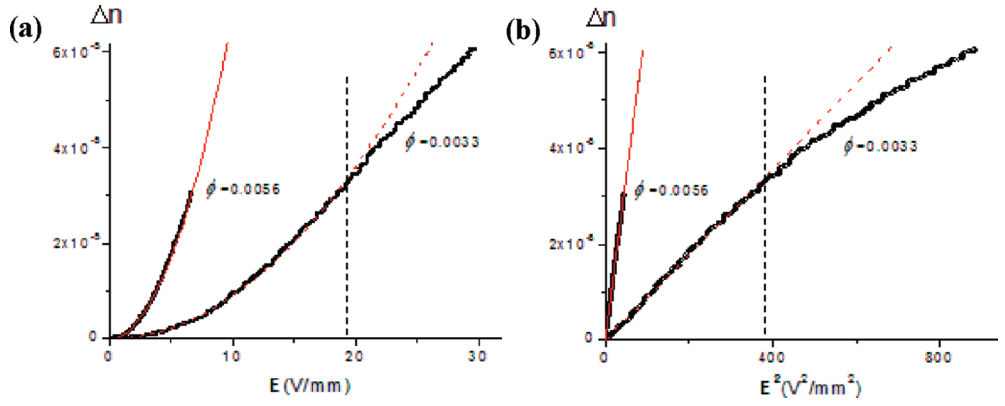

Figure 10. Induced birefringence as a function of E (a) and E^2 (b), measured by the pulsed technique in the low-field Kerr regime (the region at the left of the vertical dashed line). The lines show the best fit with the Kerr law.

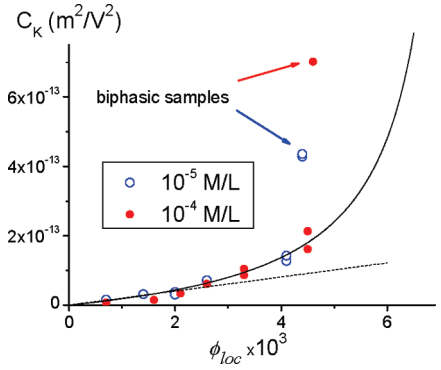

Figure 11. Kerr-coefficient of the beidellite colloidal suspensions as a function of the local volume fraction. The dashed line is the best linear fit for the data points with $\phi_{loc} < 0.0025$. The solid line is the best fit of the experimental results measured in the isotropic samples with the theoretical prediction in eq 25b, giving $\phi^* = 0.0075$.

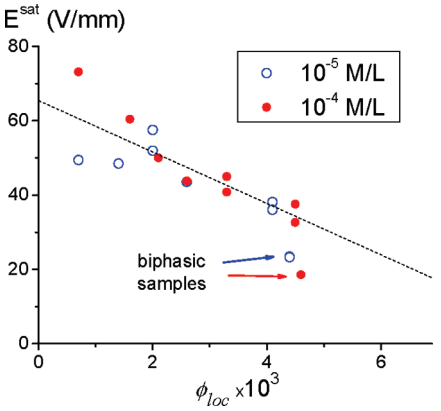

Figure 12. Saturation field of the electric birefringence as a function of the local volume fraction. The dashed line is a linear regression fit through both sets of data, excluding the biphasic samples.

studied ionic strengths of the electrolyte, showing that this parameter only has a minor influence on the electro-optic properties of the beidellite suspensions: the coupling coefficients obtained from the fit decrease only by about 20% with an increase of the ions concentration by 1 order of magnitude. This observation justifies, when needed, to treat both sets of data together, as in Figures 11 and 12 hereafter.

Valuable information about the coupling coefficient and the saturation field can be obtained also from the analysis of the electric birefringence in the weak-field Kerr regime. The curves on Figure 5, however, are poorly adapted for this purpose because they are measured manually, directly with the optical compensator, in a steady state regime under continuous sinusoidal field. Both the precision of the measurement and the limited number of points in the narrow Kerr region are not satisfying. To deal with this issue, we repeated a series of experiments on the same samples, under pulsed fields and with the more sensitive PMT detection. The applied signal is a pulse of sinusoidal field at $\nu = 500$ kHz with effective rms value $E(t)$ slowly increasing in time, as shown on Figure 9. For each sample, the rate $dE(t)/dt$ of the field variation is chosen to be very slow, compared to the reorientational relaxation time of the colloid. In this way, we are in quasi-steady state regime and the induced birefringence (Figure 9) follows adiabatically the field, with negligible time lag behind it. The plateau of $E(t)$ at the end of the pulse enables a direct experimental verification of this behavior.

A typical result is shown on Figure 10, where the induced birefringence is plotted as a function of E (Figure 10a) or E^2 (Figure 10b), E being the "instantaneous" rms field value. At low fields, Δn is proportional to E^2

$$\Delta n(E) = C_K(\phi)E^2$$

where $C_K(\phi) = (\Delta n(E)/E^2)_{E\to 0}$ is one[46] among several different definitions[19,44,47,48] of the Kerr constant in the literature. The Kerr constant $C_K(\phi)$ is quite useful for the data interpretation, as it is directly related to the coupling coefficient ΔA.[36] Indeed, substituting eqs 6 and 7 in eq 5 and developing the integrals in series for $E^2 \ll 1$, we obtain

$$C_K(\phi) = \phi\Delta n^P \left(\frac{S(E)}{E^2}\right)_{E\to 0} = \frac{\phi\Delta n^P}{15}\Delta A(\phi) \qquad (8)$$

The results for $C_K(\phi)$ are plotted as a function of the local volume fraction on Figure 11. The curve is linear at low ϕ, resulting in ϕ-independent specific Kerr-coefficient $C_K^{sp} = [C_K(\phi)/\phi]_{\phi\to 0} = -1.6 \times 10^{-11}$ m^2 V^{-2}. This gives for the experimental value of the coupling coefficient $\Delta A_{exp}(\phi \to 0) = -2.7 \times 10^{-9}$ m^2 V^{-2}, in reasonable agreement with the less

dx.doi.org/10.1021/jp201201x |J. Phys. Chem. B 2011, 115, 7751–7765

precise values obtained from the low-ϕ fits in Figure 8. When approaching the biphasic region, $C_K(\phi)$ increases considerably, due to the much more effective collective reorientation of the colloidal particles. From the result for $\phi = 0.0056$, 10^{-4} M/L, we obtain $\Delta A_{exp}(\phi_I) = -2.8 \times 10^{-8}$ m^2 V^{-2}, again in good agreement with the fit in Figure 8. We note that the precision of the measurements is lower in the biphasic region, due to the much slower reorientational relaxation times (in the seconds time-range), which makes it difficult in practice to reach the adiabatic regime.

Extrapolating the linear part of the $\Delta n(E^2)$ curve on Figure 10b up to the measured $\Delta n^{sat}(\phi)$ value, we estimate (Figure 12) the saturation field, defined as $E^{sat}(\phi) = (\Delta n^{sat}(\phi)/C_K(\phi))^{1/2}$. With decreasing volume fraction, $E^{sat}(\phi)$ increases from ~20 up to ~70 V/mm, but remains low compared with the values reported for other colloidal particles with similar volumes V^p.

Comparison with Theory. Three different physical mechanisms contribute to the reorientation of the colloidal particles under high-frequency a.c. electric field. The first one[44] is due to the dielectric contrast between the particle (ε_p) and the surrounding electrolyte (ε_e), resulting in accumulation of bound charges on the interface and in strong induced dipole moment of the particle. In a similar way, the contrast of the conductivities K_p and K_e of the two media leads to accumulation of mobile charges at the interface, i.e., to the well-known Maxwell−Wagner (MW) induced dipole moment.[49,50] The third mechanism, pointed out first by O'Konski,[47,51−53] is important for charged colloids and is related to the polarization of the ionic cloud of the particle. The large concentration of mobile counterions around the particle is equivalent to a strongly enhanced conductivity at the interface. The resulting Maxwell−Wagner−O'Konski (MWO) induced polarization is often the dominating mechanism for the particle reorientation under electric field, as well as for the strong enhancement of the dielectric permittivity[52,54−56] of the suspension.

Let us first neglect the conductivities K_p and K_e, approximating the particle as a flat (L = 0.65 nm, D = 210 nm) dielectric spheroid with $\varepsilon_p \approx 4$ (in absence of data for beidellite, we take this typical value as this discussion is not very sensitive to it) embedded in water ($\varepsilon_e \approx 80$). A uniform "external" (in the electrolyte) field with rms value E is applied to the sample. Neglecting the anisotropy of ε_p, which only plays a minor role for the extremely anisometric beidellite particles, the components of the total induced dipole moment **P** per particle are given by[28]

$$P_k = \varepsilon_0 V^p \frac{\varepsilon_e(\varepsilon_p - 1)}{\varepsilon_e + (\varepsilon_p - \varepsilon_e)N_k} E_k, \quad k = (\parallel, \perp) \tag{9}$$

where $V^p = \pi LD^2/6$ is the particle volume, the subscript k refers to the orientation of the field about the short axis of the spheroid, $N_\parallel \cong 1 - \pi L/(2D) \cong 1$ and $N_\perp = (1 - N_\parallel)/2 \cong \pi L/(4D)$ are the depolarization factors. The dielectric contribution to the internal energy of the particle, due to the interaction of the induced dipole **P** with the field and the surrounding medium, is[28]

$$U^p(\theta) = -\frac{1}{2}\frac{\varepsilon_p - \varepsilon_e}{\varepsilon_p - 1}\mathbf{E}\cdot\mathbf{P} = \text{const.} + \frac{1}{2}\varepsilon_0 V^p \frac{(\varepsilon_p - \varepsilon_e)^2}{\varepsilon_p}\mathbf{E}^2\cos^2\theta \tag{10}$$

resulting in a large dielectric contribution to the anisotropy of the excess polarizability $\Delta A = A_\parallel - A_\perp$, defined in eq 7

$$\Delta A_d = -\varepsilon_0 \frac{V^p}{kT}\frac{(\varepsilon_p - \varepsilon_e)^2}{\varepsilon_p} \tag{11}$$

However, the comparison with the experimental data shows $\Delta A_d \approx -4.6 \times 10^{-11}$ m^2 V^{-2} $\ll \Delta A_{exp}$, which means that the dielectric polarization of the particle cannot explain our results, despite the large dielectric contrast $\varepsilon_e/\varepsilon_p \gg 1$ and the extremely strong anisometry $D/L \approx 300 \gg 1$ of the beidellite sheets. We note that eq 10 holds in a large range of frequencies, from $\nu = 0$ up to $\nu \approx \nu_d$, the dielectric relaxation frequency of the two media, several orders of magnitude larger than the frequencies explored in the present study.

To calculate the MW contribution to the coupling coefficient, we will follow the approach[57−59] developed by Schwarz et al. Introducing the complex dielectric permittivities $\varepsilon_e^* = \varepsilon_e - iK_e/(\varepsilon_0\omega)$ and $\varepsilon_p^* = \varepsilon_p - iK_p/(\varepsilon_0\omega)$, where $\omega = 2\pi\nu$ is the angular frequency of the applied sinusoidal field, the potential energy of the particle is (in our notations)

$$-\frac{U^p(\theta)}{kT} = \frac{1}{2}\mathbf{E}\cdot\mathbf{A}\cdot\mathbf{E} = \text{const.} + \frac{1}{2}(A_\parallel - A_\perp)\mathbf{E}^2\cos^2\theta \tag{12a}$$

where the eigenvalues of the coupling tensor **A** are[60]

$$A_k = -\frac{\varepsilon_0 V^p}{kT} Re\left\{\tilde{\varepsilon}_e^* \frac{\varepsilon_e^* - \varepsilon_p^*}{\varepsilon_e^* + (\varepsilon_p^* - \varepsilon_e^*)N_k}\right\}, \quad k = (\parallel, \perp) \tag{12b}$$

Here the subscript k denotes, as before, the orientation of the field with respect to the (short) symmetry axis of the spheroid and $\tilde{\varepsilon}_e^* = \varepsilon_e + iKe/(\varepsilon_0\omega)$ is the complex-conjugated value of ε_e^*.

The known solution for A_k is[59−61]

$$A_k = A_k^\infty + \frac{A_k^0 - A_k^\infty}{1 + (\omega/\omega_k^{MW})^2} \tag{13}$$

where ω_k^{MW}, $k = (\parallel, \perp)$, are the MW relaxation frequencies for the two orientations

$$\omega_k^{MW} = \frac{1}{\varepsilon_0}\left|\frac{K_e + (K_p - K_e)N_k}{\varepsilon_e + (\varepsilon_p - \varepsilon_e)N_k}\right| \tag{14}$$

and A_k^0 and A_k^∞ are respectively the low ($\omega \ll \omega_k^{MW}$) and the high ($\omega \gg \omega_k^{MW}$) frequency asymptotes of the coupling coefficients

$$A_k^0 = -\frac{\varepsilon_0 V^p}{kT}\left\{\frac{\varepsilon_e + (\varepsilon_p - \varepsilon_e)N_k}{(K_e + (K_p - K_e)N_k)^2}K_e(K_e - K_p) + \frac{K_e\varepsilon_p - K_p\varepsilon_e}{K_e + (K_p - K_e)N_k}\right\} \tag{15a}$$

$$A_k^\infty = -\frac{\varepsilon_0 V^p}{kT}\frac{\varepsilon_e(\varepsilon_e - \varepsilon_p)}{\varepsilon_e + (\varepsilon_p - \varepsilon_e)N_k} \tag{15b}$$

As expected, for $\omega \gg \omega_k^{MW}$, the relevant anisotropic part of the MW coupling coefficient reduces to the dielectric contribution given in eq 11, $\Delta A^{MW} = \Delta A^\infty = \Delta A_d$, because the mobile charges

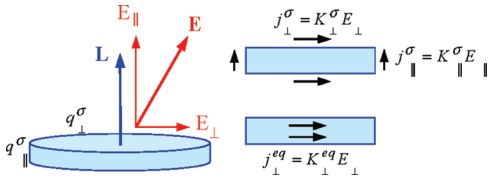

Figure 13. Schematic drawing for the estimation of the equivalent bulk conductivity of the particle K^{eq} from the surface one K^{σ}.

cannot follow the fast inversions of the applied field. At lower frequencies, the MW effect can be very strong, dominating the dielectric term by several orders of magnitude. However, taking into account that $K_p \approx 0$ and $D/L \approx 300$ for the beidellite sheets, we obtain

$$\omega_{\parallel}^{MW} \approx \frac{\pi L}{2D}\frac{K_e}{\varepsilon_0\varepsilon_p} = \frac{\pi L}{2D}\frac{\varepsilon_e}{\varepsilon_p}\omega_c \qquad (16)$$

$$\omega_{\perp}^{MW} \approx \frac{K_e}{\varepsilon_0\varepsilon_e} = \omega_c$$

where $\omega_c = 2\pi\nu_c$ is the charge relaxation frequency of the electrolyte. Because our experiments are performed at frequencies $\omega \gg \omega_c$ (to ensure a strong enough field penetration in the suspension), the MW contribution to the particle reorientation can be neglected.

Let us now consider the contribution due to the polarization of the ionic cloud around the charged beidellite particle. Long ago, O'Konski pointed out the importance of this phenomenon and proposed an elegant way[13,47,51,52] to take it into account. The large concentration of mobile counterions in the double layer at the particle/electrolyte interface results in a strong local increase of the conductivity. In the case of a thin double layer, one can treat this additional conductivity as a surface conductivity K^{σ} of the particle. This surface term renormalizes the bulk one, resulting in an equivalent conductivity of the particle

$$K_k^{eq} = K_p + \frac{K_k^{\sigma}}{\xi_k}, \quad k = (\parallel, \perp) \qquad (17)$$

where ξ_k is an effective length, depending on the particle shape and dimensions. In general, both K^{σ} and ξ are anisotropic, leading to some anisotropy of the equivalent bulk conductivity.

To obtain the MWO contribution, the equivalent conductivity K_k^{eq}, taking into account the ionic cloud polarization, should be replaced for K_p in the MW expressions given by Eqs. (13−15). For a spherical particle of radius R, with constant K^{σ} over its surface, O'Konski obtained the exact analytical result[51,52] $\xi_{\parallel} = \xi_{\perp} = R/2$ by solving the boundary value problem. He also proposed approximate solutions[52] for thin rods, flat disks and spheroids of high axial ratio. Later studies,[56,61] based on more rigorous treatment of the boundary problem for anisotropic particles, are in qualitative agreement with the O'Konski estimate, even though there is some quantitative disagreement, due to the different approximations involved.

Taking advantage from the extremely large D/L ratio of the beidellite disks, we will estimate here the MWO contribution in a simple and direct approach, without any implicit assumptions. Let us consider the beidellite particle as a thin flat circular disk with main axes L and D (Figure 13). Let the surface charge density of the particle be $q_{\perp}^{\sigma} = \text{const} < 0$ on the two flat sides and $q_{\parallel}^{\sigma}$ on the cylindrical edge side. We suppose that $q_{\perp}^{\sigma}$ and $q_{\parallel}^{\sigma}$ are of the same order of magnitude, but not necessarily equal. The counterions, needed for the neutralization of the surface charge, form a thin double layer (d_{dl} of a few nm) around the particle, with the same local surface charge density but with the opposite sign. Even though the "thin layer" condition, $d_{dl} \ll L$, is not met, we can safely consider the double layer conductivity as a surface phenomenon, i.e. we assume that the charge displacement only takes place along the surface and not normal to it. In fact, the applied field $E \sim 10^5$ V/m is very small compared to the internal field $E_{dl,\perp} \sim 10^8$ V/m across the double layer. The charge displacement normal to the surface is then negligible, compared to that along the surface under the same external field E and in absence of tangential component of the internal field $E_{dl,\parallel}$. So, the double layer behaves as a surface conductor, with essentially zero conductivity across the layer and surface conductivities $K_{\perp}^{\sigma} = \mu_{\perp}^{\sigma} q_{\perp}^{\sigma}$ and $K_{\parallel}^{\sigma} = \mu_{\parallel}^{\sigma} q_{\parallel}^{\sigma}$ respectively in the flat and edge regions of the disk. Here, $\mu_{\perp}^{\sigma}$ and $\mu_{\parallel}^{\sigma}$ are the average mobilities of the counterions in the double layer, which are expected to be lower than the mobility μ_e of the same species in the bulk electrolyte.

To estimate the equivalent conductivity $K_{\perp}^{eq}$ of the particle, we need to compare (Figure 13) the surface current density on the two flat sides $j_{\perp}^{\sigma} = K_{\perp}^{\sigma} E_{\perp}$ with the equivalent bulk current density $j_{\perp}^{eq} = K_{\perp}^{eq} E_{\perp}$ inside the disk, giving the same total current $I_{\perp} = 2j_{\perp}^{\sigma} = j_{\perp}^{eq} L$. Neglecting the small contribution of the surface edge current ($\sim L/D$ times smaller than the current on the flat side), we obtain

$$K_{\perp}^{eq} = \frac{2K_{\perp}^{\sigma}}{L} \qquad (18a)$$

In a similar way, we obtain that the edge-side equivalent conductivity

$$K_{\parallel}^{eq} = \frac{4K_{\parallel}^{\sigma}}{D} \ll K_{\perp}^{eq} \qquad (18b)$$

is $\sim 2L/D$ times smaller than $K_{\perp}^{eq}$ and can be safely neglected. We note that the simple expressions for K_k^{eq} in eq (18) are, in the high D/L limit of interest here, in excellent agreement with the results of O'Konski[52] and Saville et al.[61]

Let us now estimate the ratio $K_{\perp}^{eq}/K_e$, the equivalent "conductivity contrast" governing the MWO polarization of the ionic cloud. The density of Na^+ charges per unit area of the double layer is $q_{dl} = -q^{\sigma}$. Taking the typical value $q^{\sigma} = -0.1$ C/m^2 and assuming that the Na^+ ions have the same mobility in the double layer as in the bulk electrolyte, $\mu^{\sigma} \approx \mu_e \approx 5.2 \times 10^{-8}$ m^2/(Vs), we obtain $K^{\sigma} = \mu_e q^{\sigma} \approx 5 \times 10^{-9}$ S. This value is only an upper limit for the surface conductivity: due to a partial adsorption of the counterions on the interface and/or to higher friction in the stagnant layer, one expects $\mu^{\sigma} \le \mu_e$. Although the exact value of the ratio μ^{σ}/μ_e is still a controversial issue, recent electrokinetic and dielectric studies[62−66] suggest that the stagnant layer significantly contributes to the surface conductivity and $\mu^{\sigma}/\mu_e \approx 1$. We then expect the equivalent conductivity of the beidellite particle to be $K^{eq} = 2K^{\sigma}/L \approx 15$ S/m, an extremely large value compared to the typical bulk conductivity measured in our samples $K_e \approx 3 \times 10^{-3}$ S/m (for 10^{-4} M/L, NaCl). Roughly speaking, up to the relaxation frequency ω_k^{MWO} of the MWO effect (see below), the beidellite particle behaves as a perfect conductor immersed in a good insulator. Neglecting small terms

Table 1. Comparison of the Excess Polarizability ΔA^{sp} of Beidellite with the Data Reported for Other Strongly Anisometric Plate-Like or Rod-Like Particles[a]

particle	L (nm)	D (nm)	V^p (10^{-23} m^3)	E^{sat} (V/mm)	$\Delta\alpha(\phi\rightarrow 0)$ (10^{-29} F/m^2)	$\Delta A(\phi\rightarrow 0)$ (10^{-10} m^2/V^2)	ΔA^{sp} (10^{14} m^{-1} V^{-2})
beidellite	0.65	210	2.25	50	−1.13	−27	−1.2
laponite[69]	2	50	0.39	1000	−0.003	−0.075	−0.019
bentonite[68]	10	1200	1130	16	−12.3	−290	−0.026
	10	600	280	35	−2.6	−61	−0.022
collagen[37]	280	1.4	0.043	420	0.036	0.85	2.0
PBLG[67]	100	1.7	0.023	1000	0.006	0.15	0.66
TMV[36,53]	300	15	5.3	100	0.63	15	0.28
attapulgite[40]	3200	30	230	16	25	590	0.26
chrysotile[41]	2300	44	350	30	7.0	170	0.048
β-FeOOH[71]	230	57	39	140	0.32	7.7	0.020
gold rods[70]	190	15	3.3	100	0.63	15	0.45
	280	16	5.6	87	0.84	20	0.36
gold rods[43]	260	15	4.4	68	1.34	32	0.74

[a] The values are recalculated in our notations from the data in the cited references.

of the order of $4DK_e/(\pi LK_\perp^{eq}) \ll 1$, we obtain for the MWO excess polarizability at low-frequency

$$A_\parallel \approx \frac{\varepsilon_0 V^p}{kT}\varepsilon_e; A_\perp \approx \frac{\varepsilon_0 V^p}{kT}\frac{4D}{\pi L}\varepsilon_e \qquad (19)$$

This is exactly the result expected for *metal* particles with the same L/D ratio, dispersed in a perfect insulator with dielectric constant ε_e. For the anisotropy of the coupling coefficient, we obtain

$$\Delta A^{MWO} \approx -\frac{\varepsilon_0 V^p}{kT}\frac{4D}{\pi L}\varepsilon_e = -1.6\times 10^{-9}\ \text{m}^2\ \text{V}^{-2},$$
$$\text{for } \omega << \omega_\parallel^{MWO}, \omega_\perp^{MWO} \qquad (20)$$

This value is still lower than the experimental value $\Delta A_{exp}(\phi\rightarrow 0) = -2.7\times 10^{-9}$ m^2 V^{-2} but of the right order of magnitude. We note that, as far as $\omega \ll \omega_\parallel^{MWO}, \omega_\perp^{MWO}$, the result for ΔA^{MWO} is quite insensitive to the values of q^σ and μ^σ assumed in the above estimation.

Replacing K_k^{eq}, the equivalent conductivity of the particle, for K_p in eq 14 and again neglecting terms of the order of $4DK_e/(\pi LK_\perp^{eq}) \ll 1$, we obtain that the MWO relaxation frequencies ω_k^{MWO}

$$\omega_\parallel^{MWO} \approx \frac{K_\parallel^{eq}}{\varepsilon_0\varepsilon_p} \approx \frac{\varepsilon_e}{\varepsilon_p}\frac{K_\parallel^{eq}}{K_e}\omega_c \approx \frac{L}{2D}\frac{\varepsilon_e}{\varepsilon_p}\frac{K_\perp^{eq}}{K_e}\omega_c \sim 150\omega_c \qquad (21)$$

$$\omega_\perp^{MWO} \approx \frac{\pi L}{4D}\frac{K_\perp^{eq}}{\varepsilon_0\varepsilon_e} \approx \frac{\pi L}{4D}\frac{K_\perp^{eq}}{K_e}\omega_c \sim 15\omega_c$$

are much higher than the charge relaxation frequency ω_c of the electrolyte and are outside of the range of frequencies explored in the present experiment.

DISCUSSION

Our experimental results show that the beidellite particles are easily oriented by an electric field, with negative field-induced order parameter $S(E)$, saturating to $S^{sat} = -1/2$ at moderate fields E^{sat}. The susceptibility of the particle to the aligning action of the field is best described by the excess polarizability $\Delta A(\phi)$ (or $\Delta\alpha(\phi) = kT\Delta A(\phi)$ in absolute units), directly related to the saturating field value $E^{sat}(\phi)$

$$\Delta A(\phi) = 15\frac{S^{sat}}{E^{sat}(\phi)^2} \qquad (22)$$

where S^{sat} takes the universal value of 1 or $-1/2$, for rod-like or disk-like particles respectively.

One advantage of using $\Delta A(\phi)$, when comparing the field-induced order in different systems, is that it depends only on the coupling with the field and is independent of the particle properties probed by the specific measurement technique, e.g., electric birefringence, dichroism, light scattering, etc. However, $\Delta A(\phi)$ varies rapidly with the volume fraction ϕ of the particles, due to their excluded volume interactions. Moreover, $\Delta A(\phi)$ being directly proportional to the volume of the particle V^p, varies by several orders of magnitude from one experiment to another. For this reason, to compare our results with the literature data for other dilute suspensions of colloidal particles, we will use the specific excess polarizability, renormalized by V^p and extrapolated to $\phi = 0$

$$\Delta A^{sp} = \left.\frac{\Delta A(\phi)}{V^p}\right|_{\phi\rightarrow 0} \qquad (23)$$

We note that ΔA^{sp} still strongly depends on the dielectric constant ε_p, the surface charge density q^σ, and the aspect ratio D/L of the particle.

In Table 1, we compare our results for beidellite clay with the data reported in the literature for various, strongly anisometric, disk-like and rod-like particles in aqueous suspensions. As seen from the table, the specific excess polarizability of the beidellite particles is among the highest reported values, comparable to that of extremely thin charged rods,[37,67] a few times larger than that of the TMV,[36,53] a classical example of highly polarizable particle of similar volume V^p, and up to 2 orders of magnitude larger than the ΔA^{sp} values reported for other plate-like clay particles.[68,69] Moreover, the beidellite ΔA^{sp} value is somewhat higher than the values reported for gold rods,[43,70] expected to give ΔA^{sp} saturated to the upper limit predicted by the MW model, because of the very high bulk conductivity K_p of the particles.

All of the data presented in Table 1 are for charged particles, either dielectric or conductive, suspended in an aqueous matrix. The expected alignment mechanism in all cases is the MWO one, or the similar MW mechanism for the metal particles. The strongly enhanced response of the beidellite particles, compared to the other systems, can be explained by two main factors. The first one is the extremely thin (L = 0.65 nm) beidellite sheet, resulting in very high equivalent conductivity $K^{eq} \approx 2K^{\sigma}/L$ and effective metal-like behavior of the particle, due to $K^{eq} \gg K_e$. For the same reason, the MWO relaxation frequency is increased far beyond the frequencies used in the present experiment. The second important factor enhancing ΔA^{sp} is purely geometric: the very large aspect ratio of the particle, $D/L \approx 300$, directly enters eq 20 as a large multiplicative coefficient. Therefore, the beidellite particle orients under field like an extremely anisometric metal sheet, presenting much higher ΔA^{sp} than other oblate clay particles of the same mineralogical family, with larger sheet thickness[68] or with lower aspect ratio.[69]

Our experimental result, $\Delta A_{exp}(\phi \rightarrow 0) = -2.7 \times 10^{-9}$ m^2 V^{-2}, is even about twice larger than the theoretical limit for metal-like behavior, $\Delta A^{MWO} \approx -1.6 \times 10^{-9}$ m^2 V^{-2}. This discrepancy can be understood by considering that eq 20 holds only for monodisperse particles with diameter D. Although the size 3 beidellite sheets studied here have a quite monodisperse thickness L, their "disk diameter" D (already averaged, taking into account the polydispersity of the shape of the particles) is quite polydisperse. Estimating the size distribution function $c(D)$ from Figure 1c of ref 7, we obtain from eq 20 the theoretical limit of the average excess polarizability $\langle \Delta A^{MWO} \rangle$ for highly anisotropic ($D \gg L$) polydisperse metal particles

$$\langle \Delta A^{MWO} \rangle \approx -\frac{4\varepsilon_0 \varepsilon_e}{\pi kT} \left\langle \frac{V^p D}{L} \right\rangle = -\frac{2\varepsilon_0 \varepsilon_e}{3kT} \langle D^3 \rangle$$

$$= -2.4 \times 10^{-9} \text{m}^2 \text{ V}^{-2}$$

where the brackets indicate an average using the size distribution function $c(D)$. This value is a factor of $\langle D^3 \rangle / \langle D \rangle^3 \approx 1.49$ larger than the monodisperse value for particles with diameter $\langle D \rangle$. The experimental value is insensitive to the polydispersity of the suspension. Indeed, recasting eq 8 and averaging it with the size distribution function, we obtain

$$\langle \Delta A_{exp}(\phi \rightarrow 0) \rangle = \left\langle \left(\frac{C_K(\phi)}{\phi} \right)_{\phi \rightarrow 0} \frac{15}{\Delta n^p} \right\rangle \approx \frac{15}{\Delta n^p} C_K^{sp}$$

$$= -2.7 \times 10^{-9} \text{m}^2 \text{ V}^{-2}$$

Here we take into account the fact that the specific birefringence Δn^p depends on D only through the depolarization factors[72,73] and not directly. In our case, even the smallest particles, with $D \approx 50$ nm, present an extremely high axial ratio, $D/L > 50$, and actually Δn^p already saturates to its constant value for infinitely large disks.

After the diameter-size polydispersity correction, the agreement between the theoretical limit for metal particles and the experimental result for the beidellite sheets is quite satisfactory (about 12% difference). It is expected to be further improved by correction for the shape polydispersity of the beidellite particles, a much more difficult task which is beyond the scope of the present work.

To analyze the increase of $\Delta A_{exp}(\phi)$ with volume fraction, we need to consider the interplay of the field-induced order $S(E)$

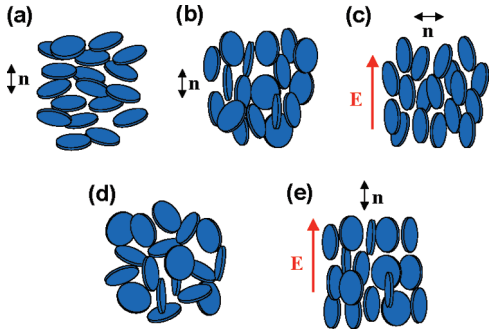

Figure 14. Spontaneous S_N and field-induced $S(E)$ orientational orders in the nematic (a−c) and the isotropic (d−e) phases of a suspension of disk-like particles. The director **n** is the macroscopic symmetry axis of the ordered phases. (a) Usual positive nematic order $S_N > 0$ in the nematic phase without field. (b) The antinematic state with $S_N < 0$, although symmetry allowed, is not an equilibrium state without field. (c) Under field, the director of the nematic phase rotates away from E. The order parameter remains positive, slightly increasing above the spontaneous value S_N. (d) Isotropic phase without field, $S_N = S(E) = 0$. (e) Para-antinematic state, with field-induced negative order $S(E) < 0$, due to the individual reorientation of the particles in a dilute isotropic phase. Upon increasing volume fraction, one expects a transition to a positive order, $S(E) > 0$, para-nematic state, similar to (c), due to the correlations between the orientations of the particles.

with the nematic orientational order S_N, spontaneously arising in the thermotropic and lyotropic liquid crystal phases of fluids comprised of strongly anisotropic molecules or colloidal particles. The nematic order, due to the orientation of the particle in the mean field of its neighbors, is described by a tensorial order parameter[27]

$$Q_{ij} = \frac{3}{2} S_N \left(n_i n_j - \frac{1}{3} \delta_{ij} \right) \quad (24)$$

Here **n** is the nematic director, a unit vector pointing along the local macroscopic symmetry axis of the phase, slowly varying in space. The scalar order parameter S_N describes the average degree of orientation of the symmetry axis of the particles along the director. Formally, S_N has the same form as $S(E)$ in eqs 5-7, provided that the external field E is replaced by the nematic mean-field,[74−76] arising from the excluded volume interactions of the particles. The symmetry axes of the particles tend to orient parallel to each other, and hence parallel to the director **n**. As a result, the spontaneous nematic order is always positive, $0.3 \leq S_N \leq 1$, regardless of the prolate or oblate shape of the particle (Figure 14a). On symmetry grounds,[27] macroscopically uniaxial phases with negative nematic order (sometimes referred to[77−79] as "anti-nematic"), are not forbidden (Figure 14b). However, the antinematic phase is never observed in real systems in absence of external fields: the state $S_N < 0$ corresponds to a saddle point of the nematic free energy[80,81] and, therefore, is not an equilibrium state.

Nematics are very sensitive to external electric and/or magnetic fields. Indeed, even for a weak coupling of the particle orientation with the field, the torque is integrated over a macroscopic number of interacting particles. Therefore, the director **n** is reoriented either along (for $\Delta A > 0$) or perpendicular to the field (for $\Delta A < 0$, Figure 14c). However, the nematic order parameter remains positive, varying only slightly[23] around its spontaneous (in zero-field) value S_N, even in the case of an

extremely strong negative coupling[82] ($-\Delta A E^2 \gg 1$). Only in the case where an imposed strong topological constraint forbids director reorientation, does the nematic order vary substantially. It may then even become negative, either locally,[83] in the vicinity of a disclination line, or transiently,[80,84] escaping from the constraint of a strong external electric field.

The situation is qualitatively different in the isotropic phase. In absence of spontaneous order and of a preferred macroscopic orientation **n**, the particles reorient independently under the action of the field. For the negative coupling case of interest here, the induced tensor order parameter

$$Q_{ij}(E) = \frac{3}{2} S(E) \left(n_i n_j - \frac{1}{3} \delta_{ij} \right)$$

is oblate, with its smallest eigenvalue along the induced director **n**, parallel to the applied field **E**. The observed positive sign of $\Delta n(E)$ (for negative Δn^P), as well as the saturation of $|S(E)|$ to 1/2, instead of 1, are direct evidence that, in strong fields, the beidellite suspensions reach the perfect antinematic order, shown on Figure 14e. Strictly speaking, the colloid is then in a para-antinematic state, as the orientational order is not spontaneous but is induced by the external field. Microscopic observations of the textures in the sample under field confirm this conclusion. In fact, in the nematic phase, the textures under field are strongly inhomogeneous:[7] the director **n** is perpendicular to the field everywhere but its orientation is degenerated in the plane normal to **E**, resulting in a strong variation of the local birefringence. In contrast, the textures observed here, in the isotropic phase under field, are highly uniform, with **n** pointing strictly along **E** and constant value of $\Delta n(E)$ over the whole observation area.

Field-induced antinematic order ($S(E) < 0$) has been reported for disk-like colloidal particles under strong electric[68,69,85] or magnetic[86,87] fields. Negative field-induced order has been observed also for rod-like particles, either with a large transverse permanent electric dipole,[46] or presenting a strong negative magnetic susceptibility.[73,77] However, the perfect antinematic ordering ($S(E) = -0.5$) of the beidellite particles under moderate fields, confirmed by the direct microscopic observation of the textures in a large range of volume fractions, from the dilute isotropic phase up to the biphasic nematic/isotropic coexistence, is quite unusual.

Let us now consider the variation of the induced order parameter with the volume fraction ϕ of the beidellite particles. Figure 8 shows a much faster increase of $-S(E)$ with the field when approaching the isotropic/nematic phase transition of the beidellite suspensions. In principle, a strong pretransitional enhancement of the susceptibility is expected close to a second-order or a weakly first-order phase transition, and it has already been reported for thermotropic liquid crystals.[27] Actually, close to a second-order transition, due to the diverging fluctuations of the spontaneous order S_N, the reorientation of a particle becomes highly correlated with its neighbors, leading to a much stronger coupling with the applied field. However, the isotropic/nematic phase transition in colloidal suspensions, mainly due to the steric hindrance mechanism of Onsager,[88] is strongly first-order, with a large jump $\Delta S_N \approx 0.8$ of the order parameter at the transition. Therefore, only weak pretransitional effects on the field-induced order should be awaited, in clear disagreement with the experimental results.

In a first approximation, the variation of $\Delta A(\phi)$ in an isotropic region with local volume fraction ϕ_{loc} is expected to be[89,90]

$$\Delta A(\phi_{loc}) = \frac{\Delta A(\phi \to 0)}{1 - \phi_{loc}/\phi^*} \tag{25a}$$

and respectively, from eq 8

$$C_K(\phi_{loc}) = \frac{C_K(\phi \to 0)}{1 - \phi_{loc}/\phi^*} \tag{25b}$$

where ϕ^* is the critical volume fraction at which the isotropic phase becomes thermodynamically unstable. By analogy with the well studied case of charged hard-rods,[91] we expect ϕ^* to be close to (or even quite larger than) the equilibrium value, $\phi_N \approx 0.006$, of the volume fraction in the nematic phase at coexistence. For the beidellite suspensions,[7] $\phi_I/\phi_N \approx 0.75$ and eq 25 predicts only a limited enhancement $\Delta A(\phi_I)/\Delta A(\phi \to 0) \approx 4$ of the excess polarizability in biphasic samples.

Figure 11 presents the best fit with eq 25b of the results for the Kerr coefficient $C_K(\phi_{loc})$ of isotropic samples, giving the reasonable value $\phi^* = 0.0075$, corresponding to an enhancement $\Delta A(\phi_I)/\Delta A(\phi \to 0) \approx 10$, about 2−3 times larger than the theoretically expected one.

The strong enhancement of the coupling coefficient, observed here for the biphasic samples of beidellite suspensions, has not been reported in previous studies of both rod-like[89,91] and disk-like[86] colloidal particles under magnetic field. For example, for isotropic and biphasic samples of gibbsite particle suspensions, van der Beek et al.[86] observed a ϕ-dependence of the Cotton−Mouton constant K_{CM} in perfect agreement with both the analytical formula in eq 25b and with a later Monte Carlo simulation study.[92] We note that our results cannot be explained by the polydispersity of the suspensions; in fact, the isotropic regions in coexistence with the nematic phase are enriched with smaller species, and $\Delta A(\phi_I)$ should decrease compared to its expected monodisperse value. Other artifacts, e.g., incomplete phase separation of the samples, with "tactoid" nematic droplets still present in the isotropic regions studied, can also be ruled out in our experiment, thanks to the direct observation of the sample texture during the measurement. We can then conclude that this discrepancy with the theoretical models is a real physical effect in the beidellite suspensions submitted to an electric field.

Another striking result of the present work is the observed enhancement of the negative field-induced order $S(E)$ by the pretransitional fluctuations of the *positive* spontaneous nematic order S_N, which is difficult to understand in the framework of available theoretical models. A speculative way to explain this strange behavior is to assume that the sample undergoes a transition between two distinct states under field. The low-field state would be para-antinematic (PAN), with uniform director $\mathbf{n} \| \mathbf{E}$ and negative order parameter $S_{PAN}(E) < 0$. The high-field state would be para-nematic with a multidomain texture (MPN), with positive order parameter $S_{MPN}(E) \approx S_N$ and nonuniform director $\mathbf{n} \perp \mathbf{E}$, randomly rotating in the sample from one domain to another one, but remaining everywhere perpendicular to **E** (as on Figure 14c). For the MPN state, the electric birefringence experiment measures an average $\langle \Delta n(E) \rangle$ value, integrated over the observation spot surface and over the sample thickness

$$\langle \Delta n(E) \rangle = -(1/2) \Delta n^P \phi S_{MPN}(E) \tag{26}$$

where the factor −1/2 comes from averaging over the random orientation of **n** in the plane normal to **E**. Formally, eq 26 is

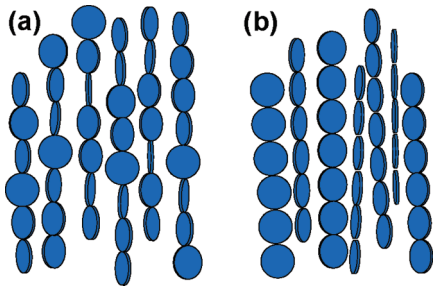

Figure 15. Azimuthal disorder in chains of disk-like particles formed under electric field. (a) The particles are disoriented within the same chain. (b) Even if the particles were aligned within each chain, the lack of correlation between the different chains would still result in an average antinematic ordering of the disks.

compatible with our results, taking into account that $S_{MPN}(E)$ saturates to $+1$, instead of $-1/2$ for the PAN-state. However, several experimental observations strongly disagree with this speculative scenario:

(a) The observation of the texture during the experiment did not reveal any substantial heterogeneity of the sample, down to the ~ 1 μm resolution limit of the optical microscope.

(b) The curves on Figure 8 are smooth functions of both E and ϕ, ruling out any discontinuous event like a possible para-antinematic to para- nematic (uniform or heterogeneous) transition.

(c) The multidomain para-nematic texture costs a large distortion energy and is energetically disfavored compared to a uniform para-nematic texture, while the electric energy gain is the same for both states. At long-term, the heterogeneous MPN state should relax to a homogeneous one, with arbitrary azimuthal orientation of the director $\mathbf{n}\perp\mathbf{E}$ and arbitrary average birefringence $0 \leq \langle\Delta n(E)\rangle \leq -\Delta n^{P}\phi S(E) \approx -\Delta n^{P}\phi$. This prediction strongly disagrees with both the measured birefringence values and the texture observations over times up to several hours.

Yet another possible explanation of the observed pretransitional behavior might be a field-induced organization of the beidellite disks into chains, as already observed for other colloidal systems.[85,93,94] Indeed, for volume fractions approaching the isotropic/nematic transition of the suspension, the interparticle separation is of the order of the disk diameter D and the induced dipoles strongly interact, which may favor the growth of chains of particles, with the chain axis **C** along the field direction (Figure 15). In the chain, the symmetry axes **L** of the disks are perpendicular to **C**, but there is no physical reason to expect them to point in the same direction, either inside the same chain (Figure 15a), or from one chain to another (Figure 15b). In that case, the observed birefringence will still follow eq 26, with field-induced antinematic orientational order, as experimentally observed, described by $S < 0$, $S^{sat} = -1/2$, and the nematic director **n** parallel to the field **E** and to the chain axis **C**. However, the chain reorientation under field would now be a collective process, under the much stronger torque integrated over all the particles in the chain, explaining the observed fast increase of the coupling coefficient $\Delta A(\phi)$ close to the biphasic domain. A detailed electro-optic study of the pretransitional domain, in combination with small-angle X-ray scattering experiments under electric field, is in progress in order to test this chain-forming scenario.

CONCLUSIONS

We described here an electric birefringence experiment optimized for the study of the field-induced orientational order in aqueous suspensions of colloidal particles. The traditional Kerr cell is replaced by a thin flat sample, sealed in an optical capillary. A high frequency a.c. electric field is applied along the capillary axis by two external electrodes. This fairly original experimental geometry prevents the electrochemical degradation of the sample, minimizes heating and convection artifacts, and enables a direct microscopic observation of the textures throughout the experiment. Moreover, it ensures a better field propagation inside the suspension than when the field is applied normal to the flat walls of the capillary.

We studied the field-induced birefringence in the isotropic phase of aqueous suspensions of exfoliated natural beidellite clay particles that are ($L = 0.65$ nm) thin flat charged sheets with high aspect ratio, $D/L \approx 300$. In isotropic ($\phi < 0.0042$) and biphasic ($0.0042 < \phi < 0.0059$) samples, we observed a strong field-induced birefringence $\Delta n(E)$, saturating at moderate E^{sat} field to a plateau Δn^{sat} proportional to the volume fraction ϕ. The field-induced order parameter $S(E)$ is negative and saturates to $S^{sat} = -0.5$ above E^{sat}. This corresponds to a perfect "anti-nematic" order of the beidellite particles; that is, the disk normals are perpendicular to the field, without any preferred azimuthal direction. The particles are strongly aligned by the electric field and the measured specific excess polarizability ΔA^{sp} is among the highest data reported for other suspensions of strongly anisometric dielectric and metal particles.

With a simple model, we showed that the high ΔA^{sp} value observed is in good agreement with the MWO polarization mechanism, i.e., with a strong induced polarization of the electrical double layer of counterions at the particle/water interface. The estimated equivalent conductivity of the beidellite particle $K^{eq} = 2K^{\sigma}/L$ is several orders of magnitude larger than the bulk conductivity of the electrolyte K_e. The resulting metal-like behavior of the beidellite disks under field is expected to persist up to $\nu \approx 10$ MHz, beyond the frequency range of the present experiment.

In the isotropic regions of biphasic nematic/isotropic samples, the excess polarizability further increases by an order of magnitude, showing collective reorientation of the particles under field. Qualitatively, this behavior is likely to result from the coupling of the field-induced order $S(E)$ with the pretransitional fluctuations of the nematic order S_N that spontaneously appears above the isotropic/nematic transition of the colloidal suspension. However, how the negative induced order, $S(E) < 0$, is enhanced by the fluctuations of the strongly positive spontaneous one, $S_N \approx 0.8$, remains an open question.

We also propose that the enhanced interactions of the particles with the field at high volume fractions might be due to the formation of chains of particles, with average antinematic order of the beidellite disks in the same chain, or from one chain to another. X-ray scattering experiments under in situ applied electric field are planned in order to test this possible arrangement of the beidellite disks in chains.

ACKNOWLEDGMENT

Authors gratefully acknowledge the financial support from the ANR (Agence Nationale de la Recherche, "programme blanc" ANISO) and from the Lorraine Region, France.

REFERENCES

(1) Odom, I. E. *Phil. Trans. R. Soc. London A* **1984**, *311*, 391.
(2) Harvey, C. C.; Lagaly, G. In *Handbook of clay science*; Bergaya, F., Theng, B. G., Lagaly, G., Eds.; Elesivier: New York, 2006; Chapter 10.1.
(3) Langmuir, I. *J. Chem. Phys.* **1938**, *6*, 873.
(4) Michot, L. J.; Bihannic, I.; Maddi, S.; Funari, S. S.; Baravian, C.; Levitz, P.; Davidson, P. *Proc. Natl. Acad. Sci. U.S.A.* **2006**, *103*, 16101.
(5) Michot, L. J.; Bihannic, I.; Maddi, S.; Baravian, C.; Levitz, P.; Davidson, P. *Langmuir* **2008**, *24*, 3127.
(6) Michot, L. J.; Paineau, E.; Bihannic, I.; Maddi, S.; Duval, J. F. L.; Baravian, C.; Davidson, P.; Levitz, P. *Clay Miner.* **2011**in press.
(7) Paineau, E.; Antonova, K.; Baravian, C.; Bihannic, I.; Davidson, P.; Dozov, I.; Imperor-Clerc, M.; Levitz, P.; Madsen, A.; Meneau, F.; Michot, L. J. *J. Phys. Chem. B* **2009**, *113*, 15858.
(8) Gabriel, J. C. P.; Davidson, P. *Adv. Mater.* **2000**, *12*, 9.
(9) Davidson, P.; Gabriel, J. C. P. *Curr. Opin. Colloid Interface Sci.* **2005**, *9*, 377.
(10) Kerr, J. *Philos. Mag. Ser. IV* **1875**, *50*, 337.
(11) Lauffer, M. A. *J. Am. Chem. Soc.* **1939**, *61*, 2412.
(12) Heller, W. *Rev. Mod. Phys.* **1942**, *14*, 0390.
(13) O'Konski, C. T.; Zimm, B. H. *Science* **1950**, *111*, 113.
(14) Fredericq, E.; Houssier, C. *Electric dichroism and electric birefringence*; Clarendon Press: Oxford, 1973.
(15) O'Konski, C. T. *Molecular electro-optics*; M. Dekker: New York, 1976.
(16) Stoylov, S. P.; Stoimenova, M. V. *Molecular and colloidal electro-optics*; CRC/Taylor & Francis: Boca Raton, FL, 2007.
(17) O'Konski, C. T.; Haltner, A. J. *J. Am. Chem. Soc.* **1956**, *78*, 3604.
(18) Jennings, B. R.; Brown, B. L.; Plummer, H. *J. Colloid Interface Sci.* **1970**, *32*, 606.
(19) Knudsen, A. W. *Am. J. Phys.* **1975**, *43*, 888.
(20) Stoylov, S. P. *Colloid electro-optics: theory, techniques, applications*; Academic Press: San Diego, CA, 1991.
(21) Stellwagen, N. C. *Biopolymers* **1991**, *31*, 1651.
(22) Baily, E. D.; Jennings, B. R. J. *Colloid Interface Sci.* **1973**, *45*, 177.
(23) Lelidis, I.; Nobili, M.; Durand, G. *Phys. Rev. E* **1993**, *48*, 3818.
(24) Forget, S.; Dozov, I.; Martinot-Lagarde, P. *Mol. Cryst. Liq. Cryst. Sci. Technol. Sect. A-Mol. Cryst. Liq. Cryst.* **1999**, *329*, 1217.
(25) Lamarque-Forget, S.; Pelletier, O.; Dozov, I.; Davidson, P.; Martinot-Lagarde, P.; Livage, J. *Adv. Mater.* **2000**, *12*, 1267.
(26) Lamarque-Forget, S.; Martinot-Lagarde, P.; Dozov, I. *Jpn. J. Appl. Phys. Part 2 - Lett.* **2001**, *40*, L349.
(27) De Gennes, P.-G.; Prost, J. *The physics of liquid crystals*, 2nd ed.; Clarendon Press: Oxford, 1993.
(28) Landau, L. D.; Lifshitz, E. M. *Electrodynamics of continuous media*; Pergamon Press: Oxford, 1960.
(29) Jackson, J. D. *Classical electrodynamics*; Wiley: New York, 1962.
(30) Demirörs, A. F.; Johnson, P. M.; van Kats, C. M.; van Blaaderen, A.; Imhof, A. *Langmuir* **2010**, *26*, 14466.
(31) Kang, K.; Dhont, J. K. G. *Eur. Phys. J. E* **2009**, *30*, 333.
(32) Kang, K.; Dhont, J. K. G. *Soft Matter* **2010**, *6*, 273.
(33) Adaptive mesh finite element solution, using the FlexPDE 6 evaluation version from PDE Solutions Inc.; www.pdesolutions.com.
(34) Watson, J. H. L.; Heller, W.; Wojtowicz, W. *J. Chem. Phys.* **1948**, *16*, 997.
(35) Livage, J.; Pelletier, O.; Davidson, P. *J. Sol-Gel Sci. Technol.* **2000**, *19*, 275.
(36) O'Konski, C. T.; Yoshioka, K.; Orttung, W. H. *J. Phys. Chem.* **1959**, *63*, 1558.
(37) Yoshioka, K.; O'Konski, C. T. *Biopolymers* **1966**, *4*, 499.
(38) Schwarz, G.; Schrader, U. *Biopolymers* **1975**, *14*, 1181.
(39) Morris, V. J.; Jennings, B. R. *J. Colloid Interface Sci.* **1978**, *66*, 313.
(40) Fairey, R. C.; Jennings, B. R. *J. Colloid Interface Sci.* **1982**, *85*, 205.
(41) Isherwood, R.; Jennings, B. R. *J. Colloid Interface Sci.* **1985**, *108*, 462.
(42) Jennings, B. R.; Nash, M. *J. Colloid Interface Sci.* **1989**, *131*, 47.
(43) Zhivkov, A. M.; Van der Zande, B. M. I.; Stoylov, S. P. *Colloid Surf. A-Physicochem. Eng. Asp.* **2002**, *209*, 299.
(44) Peterlin, A.; Stuart, H. A. *Z. Phys.* **1939**, *112*, 129.
(45) Mantegazza, F.; Bellini, T.; Degiorgio, V.; Delgado, A. V.; Arroyo, F. J. *J. Chem. Phys.* **1998**, *109*, 6905.
(46) Thurston, G. B.; Bowling, D. I. *J. Colloid Interface Sci.* **1969**, *30*, 34.
(47) O'Konski, C. T.; Haltner, A. J. *J. Am. Chem. Soc.* **1957**, *79*, 5634.
(48) Mantegazza, F.; Bellini, T.; Buscaglia, M.; Degiorgio, V.; Saville, D. A. *J. Chem. Phys.* **2000**, *113*, 6984.
(49) Maxwell, J. C. *A treatise on electricity and magnetism*, Unabridged 3d ed.; Dover Publications: New York, 1954.
(50) Wagner, K. W. *Arch. Elecktro. Technol.* **1914**, *2*, 371.
(51) O'Konski, C. T. *J. Chem. Phys.* **1955**, *23*, 1559.
(52) O'Konski, C. T. *J. Phys. Chem.* **1960**, *64*, 605.
(53) O'Konski, C. T.; Krause, S. *J. Phys. Chem.* **1970**, *74*, 3243.
(54) Schwan, H. P.; Schwarz, G.; Maczuk, J.; Pauly, H. *J. Phys. Chem.* **1962**, *66*, 2626.
(55) Fixman, M. *J. Chem. Phys.* **1980**, *72*, 5177.
(56) Bertrand, E. A.; Endres, A. L. *J. Chem. Phys.* **2009**, *130*, 224705.
(57) Schwarz, G. *J. Chem. Phys.* **1963**, *39*, 2387.
(58) Schwarz, G.; Saito, M.; Schwan, H. P. *J. Chem. Phys.* **1965**, *43*, 3562.
(59) Saito, M.; Schwan, H. P.; Schwarz, G. *Biophys. J.* **1966**, *6*, 313.
(60) Foster, K. R.; Osborn, A. J.; Wolfe, M. S. *J. Phys. Chem.* **1992**, *96*, 5483.
(61) Saville, D. A.; Bellini, T.; Degiorgio, V.; Mantegazza, F. *J. Chem. Phys.* **2000**, *113*, 6974.
(62) Lyklema, J. *J. Phys.-Condes. Matter* **2001**, *13*, 5027.
(63) Lyklema, J. *Fundamentals of interface and colloid science*; Academic Press: San Diego, CA, 2000.
(64) Jimenez, M. L.; Arroyo, F. J.; Carrique, F.; Kaatze, U.; Delgado, A. V. *J. Colloid Interface Sci.* **2005**, *281*, 503.
(65) Carrique, F.; Arroyo, F. J.; Shilov, V. N.; Cuquejo, J.; Jimenez, M. L.; Delgado, A. V. *J. Chem. Phys.* **2007**, 126.
(66) Jimenez, M. L.; Arroyo, F. J.; Carrique, F.; Delgado, A. V. *J. Colloid Interface Sci.* **2007**, *316*, 836.
(67) Yamaoka, K.; Yamamoto, S.; Ueda, K. *Biopolymers* **1987**, *26*, 673.
(68) Shah, M. J.; Hart, C. M.; Thompson, D. C. *J. Phys. Chem.* **1963**, *67*, 1170.
(69) Zhivkov, A. M.; Stoylov, S. P. *Colloid Surf. A-Physicochem. Eng. Asp.* **2002**, *209*, 315.
(70) Van der Zande, B. M. I.; Koper, G. J. M.; Lekkerkerker, H. N. W. *J. Phys. Chem. B* **1999**, *103*, 5754.
(71) Peikov, V.; Sasai, R.; Tanilgawa, M.; Petkanchin, I.; Yamaoka, K. J. *Colloid Interface Sci.* **2006**, *295*, 445.
(72) Neveu-Prin, S.; Tourinho, F. A.; Bacri, J. C.; Perzynski, R. *Colloids Surf., A* **1993**, *80*, 1.
(73) Lemaire, B. J.; Davidson, P.; Ferre, J.; Jamet, J. P.; Petermann, D.; Panine, P.; Dozov, I.; Jolivet, J. P. *Eur. Phys. J. E* **2004**, *13*, 291.
(74) Maier, W.; Saupe, A. *Z. Naturforsch., A: Astrophys. Phys. Phys. Chem.* **1958**, *13*, 564.
(75) Maier, W.; Saupe, A. *Z. Naturforsch., A: Astrophys. Phys. Phys. Chem.* **1959**, *14*, 882.
(76) Maier, W.; Saupe, A. *Z. Naturforsch., A: Astrophys. Phys. Phys. Chem.* **1960**, *15*, 287.
(77) Lemaire, B. J.; Davidson, P.; Ferre, J.; Jamet, J. P.; Petermann, D.; Panine, P.; Dozov, I.; Stoenescu, D.; Jolivet, J. P. *Faraday Discuss.* **2005**, *128*, 271.
(78) Meheust, Y.; Knudsen, K. D.; Fossum, J. O. *J. Appl. Crystallogr.* **2006**, *39*, 661.
(79) Avendano, C.; Muller, E. A. *Phys. Rev. E* **2009**, 80.
(80) Martinot-Lagarde, P.; Dreyfus-Lambez, H.; Dozov, I. *Phys. Rev. E* **2003**, 67.
(81) Fournier, J. B.; Galatola, P. *EPL* **2005**, *72*, 403.
(82) Dhara, S.; Madhusudana, N. V. *Eur. Phys. J. E* **2007**, *22*, 139.

(83) Schopohl, N.; Sluckin, T. J. *Phys. Rev. Lett.* **1987**, *59*, 2582.
(84) Barberi, R.; Ciuchi, F.; Durand, G. E.; Iovane, M.; Sikharulidze, D.; Sonnet, A. M.; Virga, E. G. *Eur. Phys. J. E* **2004**, *13*, 61.
(85) Rozynek, Z.; et al. *J. Phys.: Condensed Matter* **2010**, *22*, 324104.
(86) van der Beek, D.; Petukhov, A. V.; Davidson, P.; Ferre, J.; Jamet, J. P.; Wensink, H. H.; Vroege, G. J.; Bras, W.; Lekkerkerker, H. N. W. *Phys. Rev. E* **2006**, *73*, 041402.
(87) Hemmen, H.; Ringdal, N. I.; De Azevedo, E. N.; Engelsberg, M.; Hansen, E. L.; Méheust, Y.; Fossum, J. O.; Knudsen, K. D. *Langmuir* **2009**, *25*, 12507.
(88) Onsager, L. *Ann. N.Y. Acad. Sci.* **1949**, *51*, 627.
(89) Fraden, S.; Maret, G.; Caspar, D. L. D.; Meyer, R. B. *Phys. Rev. Lett.* **1989**, *63*, 2068.
(90) Vroege, G. J.; Lekkerkerker, H. N. W. *Rep. Prog. Phys.* **1992**, *55*, 1241.
(91) Fraden, S.; Maret, G.; Caspar, D. L. D. *Phys. Rev. E* **1993**, *48*, 2816.
(92) de Azevedo, E. N.; Engelsberg, M. *Langmuir* **2009**, *25*, 1175.
(93) Halsey, T. C.; Toor, W. *Phys. Rev. Lett.* **1990**, *65*, 2820.
(94) Parmar, K. P. S.; Meheust, Y.; Schjelderupsen, B.; Fossum, J. O. *Langmuir* **2008**, *24*, 1814.